

CrossMark  
click for updatesCite this: *J. Mater. Chem. C*, 2015, 3,  
995

## Nanoindentation studies to separate thermal and optical effects in photo-softening of azo polymers

James M. Harrison,<sup>ab</sup> Dina Goldbaum,<sup>b</sup> T. Christopher Corkery,<sup>a</sup>  
Christopher J. Barrett<sup>\*a</sup> and Richard R. Chromik<sup>\*b</sup>

Mechanical characterization of an azobenzene dye-containing polymer (p4VP(DY7)<sub>0.50</sub>) by nanoindentation shows a significant photo-softening effect under visible irradiation at 532 nm. Both strong rate-dependent plastic softening, as well as a rate-independent elastic modulus decrease are observed. Indentation at elevated, sub-glass transition temperatures results in only a rate-independent decrease in hardness however. These findings indicate, from a mechanics standpoint, for the first time a distinct mechanism for the photomechanical softening in azo-materials that is different from a simple thermal effect. The main hallmark of the photosoftening effect was significant viscoplastic flow with strong rate dependence. The presence of the viscoplastic softening in azo-polymers was accounted for in analysis of nanoindentation data to obtain an accurate elastic modulus unaffected by the presence of creep in the unloading curves. These results provide considerable insight into the long-observed and long-debated mechanism of all-optical surface patterning below  $T_g$ .

Received 16th October 2014  
Accepted 29th November 2014

DOI: 10.1039/c4tc02336f

www.rsc.org/MaterialsC

### Introduction

Azobenzene-containing polymer thin films possess the well-known ability for all-optical single step surface patterning, for example to form surface relief gratings (SRGs) under visible light irradiation.<sup>1,2</sup> These materials exhibit significant macroscopic mass transport under inhomogeneous irradiation, and have been engineered to optimize SRG formation and surface patterning for a variety of optical material applications.<sup>3–5</sup> Under irradiation, some azobenzene chromophores initially in their *trans* geometric isomer will be converted to their *cis* state, from which they will thermally reconvert to the thermodynamically favourable *trans* state again over time. The macroscopic mechanical effects of irradiation are a function of the continuous *trans-cis-trans* photoisomerization cycling of azobenzene.<sup>6</sup> All of this optical patterning can be performed readily at room temperature, well below the expected  $T_g$  of the glassy materials, and the mechanism for this unexpected process has been in debate for 20 years since the first reports. However, this mechanical cycling has been implicated in a change in elastic modulus and/or viscosity, which is expected for a system to achieve such significant light-induced flow, well below the bulk  $T_g$ .

As one of the currently leading mechanisms for this curious process, it has been proposed that pressure gradients, due to

differences in the free volume of the azobenzene chromophore in the *trans* and *cis* configurations, are responsible for the mass transport.<sup>7,8</sup> By this model viscoelastic flow is produced due to the *cis*-isomer's higher free space requirements, and agrees well with experiment, and implies a viscosity under irradiation significantly lower than that in the dark.<sup>3</sup> Other mechanisms include that of Pederson *et al.*, who developed a model based on photoinduced reorientation and optical anisotropy in liquid crystalline side-chain polymers to explain the long term stability of the *trans-cis* isomerization.<sup>9</sup> This model, however, contradicts experimental results in amorphous polymers.<sup>10</sup> Lefin *et al.* also proposed a diffusion model, which associates the mass transport with photoinduced translation along the long axis in the azobenzene molecules.<sup>11</sup> The development of a model based on the moving-particle semi-implicit method by Barada *et al.* suggested the gradient force of the optical electric field and the influence of surface tension as the primary forces responsible for SRG formation.<sup>12</sup> A statistical approach developed by Juan *et al.* allowed the prediction of complex mass transport under different illumination conditions and operates under the assumption that local temperatures are near the glass transition temperature  $T_g$ .<sup>10</sup> More work is necessary to establish a fundamental model that agrees with all experiments, and so much work has been done to analyze azo-materials both from a fundamental mechanical level, as well as modelling the bulk mechanical properties at various scales.

Thermally induced SRG formation was proposed by Ram-anujam and co-workers, which was subsequently examined by Leopold *et al.*<sup>13,14</sup> By examining diffraction efficiency as a function of pulse intensity, they define an energy volume density

<sup>a</sup>Department of Chemistry, McGill University, Otto Maass Building, 801 Sherbrooke St. W, Montreal, Quebec, H3A 0B8, Canada. E-mail: christopher.barrett@mcgill.ca

<sup>b</sup>Department of Mining and Materials Engineering, McGill University, M. H. Wong Building, 3610 University St., Montreal, Quebec, H3A 0C5, Canada. E-mail: richard.chromik@mcgill.ca

threshold above which the efficiency quickly approaches its maximum value. This threshold is useful as it corresponds to the energy above which thermally driven SRG formation occurs. In further work, Baldus and Leopold *et al.* determined the threshold of absorbed energy above which SRG formation occurs.<sup>15</sup> They go on to develop a model predicting thermal SRG formation for thermal gratings. These works indicate that SRG formation is not necessarily strictly a photomechanical phenomenon, and indeed in some cases it is independent of azobenzene photoisomerization. Any thermal model however, has yet to address the pervasive and conflicting set of experiments that only isomerizing azo dyes are able to be photo-patterned, and not any of the absorbing or non-isomerizing dyes with similar absorbance and thermal properties. Previous work toward understanding photomechanically driven pattern formation has generally assumed both the viscosity and modulus of the polymer was significantly reduced when exposed to light, yet actual measurements of this had yet to be reported. Saphiannikova *et al.* assumed that under illumination the polymer film undergoes considerable plastification, reducing the polymer elastic modulus by more than three orders of magnitude.<sup>16</sup> Karageorgiev *et al.* determined that a more moderate modulus change occurred in pDR1m films, from 3.4 GPa to 0.9 GPa under 60 mW cm<sup>-2</sup> 532 nm circularly polarized irradiation.<sup>17</sup> They further noted a light-induced viscosity several orders of magnitude smaller than the typical viscosity of the polymer in a glassy state. This moderate change in modulus coupled with a very large change in viscosity implies a softening method that must be photomechanical in nature, as opposed to thermally driven. They also distinguished between photomechanical processes and thermal processes by showing there exists directional viscoelastic flow parallel to the polarization of the light source. However, Richter, Nowicki, and Wolf have shown a modulus increase in pDR1m films under 10 mW cm<sup>-2</sup> 532 nm irradiation.<sup>18</sup> They measured a modulus increase from 5.0 GPa to 6.0–6.7 GPa, depending on the length of time for which the sample was irradiated. It is possible that different experimental procedures are likely for the divergent results under similar experimental conditions.

Lee and White determined, by use of thermal camera, that the temperature increase in irradiated monodomain azobenzene liquid crystalline network samples can be split into two regimes: “photochemical”, when the light intensity is less than approximately 100 mW cm<sup>-2</sup>, and “photochemical and photo-thermal”, where the intensity is above this threshold.<sup>19</sup> In the photochemical regime, the heating effect of the light is less than 3 K; this temperature increase has also been determined computationally,<sup>20</sup> but little work has been done to precisely characterize the bulk mechanical properties of azo-polymer samples under both direct heating and moderate intensity irradiation. Vapaavuori and Mahimwalla *et al.* showed that under 15 mW cm<sup>-2</sup> irradiation, the strain rate sensitivity of pDR1a, the first and most commonly employed azo-polymer for all-optical patterning, and poly(4-vinylpyridine) (p4VP), doped with disperse yellow 7 (DY7) at a complexation degree of 0.50, increased by 81% and 123% respectively.<sup>21</sup> However, they failed to isolate time-invariant mechanical parameters corresponding

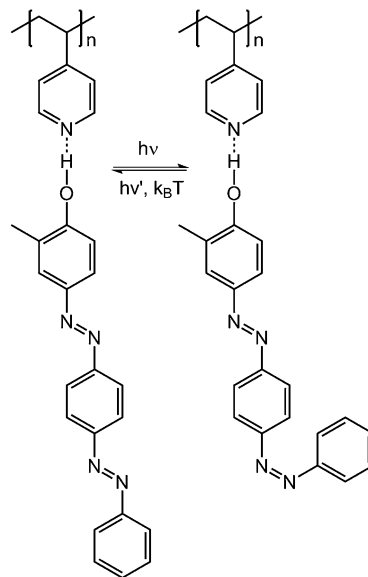


Fig. 1 Disperse yellow 7 doped poly(4-vinylpyridine). The azobenzene chromophores isomerize from the *trans* to the *cis* state photochemically. The reversion may also be induced photochemically, or the chromophore will thermally relax to the thermodynamically favourable *trans* state.

to spring and slider (elastic and plastic) elements in a traditional spring-dashpot-slider mechanical model. In this paper, we present a characterization of DY7-doped p4VP under 15 mW cm<sup>-2</sup> irradiation, as well as examine the changes in mechanical properties, strictly as a function of temperature. Examined here is p4VP at both a large and small complexation degree: 0.50 (p4VP(DY7)<sub>0.50</sub>) and 0.01 (p4VP(DY7)<sub>0.01</sub>) (Fig. 1). These complexation degrees indicate that a chromophore is paired with a repeat unit of the polymer every second and every hundredth unit respectively. These samples were chosen as it has been found that the efficiency of SRG formation is largest for a complexation degree of 0.50. Strain rate sensitivity changes were examined as a function of both irradiation and due to a temperature increase below the glass transition. Under both conditions, we also examine the elastic modulus as well as the material hardness. We further discuss the implications of the activated creep mechanism on the elastic modulus measurements, and how this provides new insight into the long-controversial mechanism of all-optical patterning below  $T_g$ .

## Experimental

### Materials

Two p4VP(DY7) samples were prepared at complexation degrees of 0.01 and 0.50. These samples were prepared by dissolving p4VP (Polymer Source, Inc.,  $M_w = 5400 \text{ g mol}^{-1}$ ) and DY7 (Sigma-Aldrich, 95%) in THF, stirring 24 hours, and drop casting onto silicon substrates. The samples were annealed at 120 °C and 135 °C respectively for 72 h under vacuum.

## Nanoindenter

Nanoindentation was performed using a Hysitron TI 900 TriboIndenter. Experiments were performed using Hysitron's xSol High Temperature Stage and the corresponding high temperature indentation tip. A standard calibration procedure using fused quartz was performed. Indentation was then performed on the azo-polymer samples under three conditions: standard, elevated temperature, and under irradiation. These conditions will be referred to as "Reference", "50 °C", and "15 mW cm<sup>-2</sup>" respectively. Reference conditions refer to indents performed at ambient lab temperature (23 °C) with no directly incident light. Indents performed under "50 °C" conditions were held at 50 °C with no incident light, where the stage was allowed to equilibrate for 30 minutes before indentation began. The "15 mW cm<sup>-2</sup>" conditions refer to indentations performed with the sample under direct irradiation from a 15 mW cm<sup>-2</sup> 532 nm solid state laser (B & W Tek 300 mW cm<sup>-2</sup> laser passed through a neutral density filter). For each of the conditions, indentation was performed at five different loading rates: 50, 100, 200, 500 and 1000 μN s<sup>-1</sup>, to a maximum load of 1000 μN. At each loading rate 25 indents were performed in a 5 by 5 grid, in which all indents were separated from each other by 30 μm. The rates of loading and unloading were the same, and for each indent there was a 60 second hold period at maximum load. The loading curves and an example load-depth curve can be seen in Fig. 2.

## Hardness

Hardness was determined by

$$H = \frac{P}{A} \quad (1)$$

as described by Oliver and Pharr, where  $P$  is the load and  $A$  is the projected contact area.<sup>22</sup> The contact area is calculated as a function of the contact depth,

$$h_c = h_{\max} - \varepsilon \frac{P}{S} \quad (2)$$

in which  $\varepsilon$  is a term related to indenter geometry. The indenter depth at the beginning of the hold period,  $h_{\max}$ , was used so as to minimize the effect of viscoplastic drift and solely model the time-invariant plastic element. This correction is imperfect, as there is a small viscosity effect which is influencing the measurement. However, the effect is very small in all cases other than the irradiated high azo sample. The stiffness,  $S$ , was defined by Oliver and Pharr as the derivative

$$S = \left. \frac{dP}{dh} \right|_{h=h_{\max}}$$

of the power-law unloading fit,<sup>22</sup>

$$P = A(h - h_i)^m. \quad (3)$$

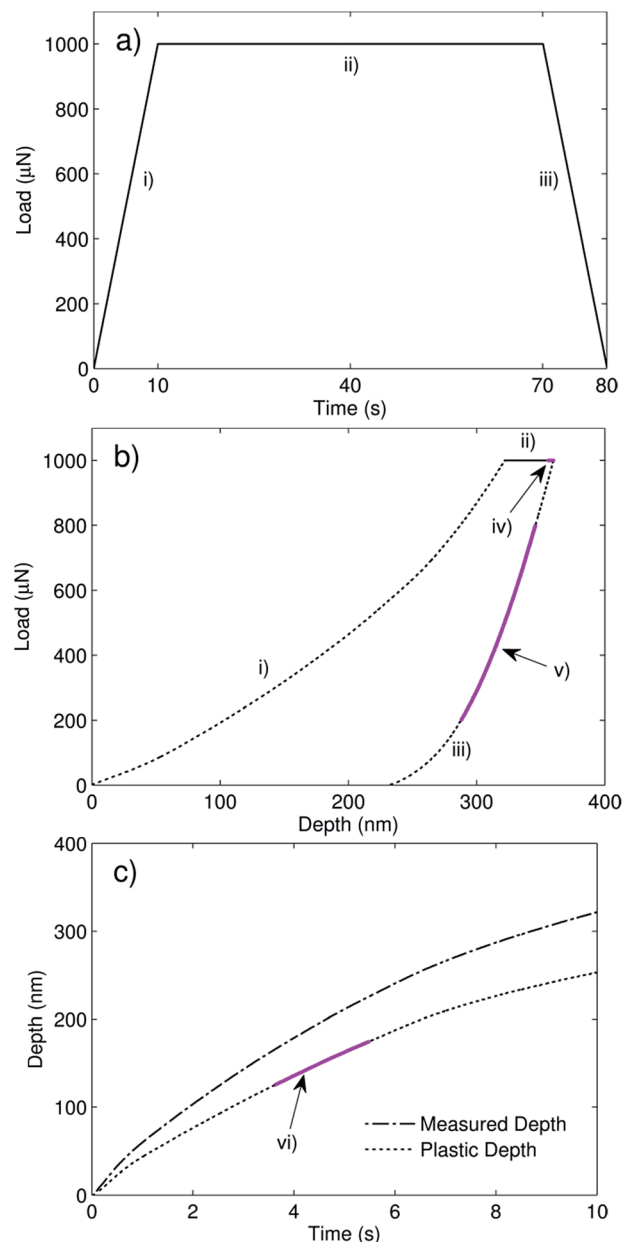


Fig. 2 Example plots of (a) the load function, (b) the load-depth curve, and (c) depth and plastic depth vs. time. (a) and (b) are plotted over the entire loading-hold-unloading process, whereas (c) is only plotted over the loading segment. Regions (i), (ii), and (iii) indicate the loading, hold, and unloading segments of the indentation respectively. Emphasized region (iv) indicates the period over which the residual hold displacement  $h_h$  was measured for the creep-corrected modulus. The hardness was measured at maximum displacement (at the end of the hold period). Region (v) indicates the range over which the Oliver and Pharr power law was fit. Region (vi) is the range over which the constant rate of loading strain rate sensitivity was determined.

## Elastic modulus

The most common method for calculating elastic modulus from nanoindentation comes from the method of Oliver and Pharr in which the power law relation is fit to the unloading

curve.<sup>22</sup> The reduced modulus can be determined by Sneddon's elastic contact solution<sup>23</sup>

$$E_r = \frac{\sqrt{\pi}}{2} \frac{S}{\sqrt{A_c}} \quad (4)$$

The impact of creep in nanoindentation has been noted in several studies and it can be especially pronounced in polymers.<sup>24–27</sup> The creep can be examined in primary and secondary segments at constant load (Fig. 3).<sup>28</sup> The primary region is the most significant for the measurement of modulus, and is typified by rapid descent under constant load. The effects of this primary region can typically be avoided by using a hold period at maximum load before unloading. The secondary segment is typified by a near-constant descent under constant load. Although a hold period may be effective at eliminating the effects of the primary creep regime, this secondary regime is uncorrected and can significantly affect determination of the elastic modulus from unloading curves when unloading rates are slow. In this paper, the method developed by Ngan *et al.* was applied to determine the elastic modulus corrected for viscoelastic creep, which should be independent of time or indentation rate.<sup>19</sup>

In a series of papers, Ngan and co-workers developed a model to correct for linear viscoelastic creep by using a superposition approximation in which the indenter displacement  $h$  is the sum of the creep component and the elastic component.<sup>19,29–32</sup> This model necessitates the use of a hold period at maximum load, during which it is possible to measure the creep rate. They further developed a model to correct for viscoelastic creep in a general power law form, where it is assumed the load can vary during a hold period. They verified this model computationally and experimentally, by finite element methods and indentation on amorphous selenium. For the purpose of this investigation, the linear creep correction model is used as closed-loop load control of the indenter ensuring that there is

no variation in load during the hold period. The method defines a corrected effective stiffness

$$S_e = \left( \frac{1}{S} - \frac{\dot{h}_h}{\dot{P}_u} \right)^{-1} \quad (5)$$

where  $\dot{h}_h$  is the tip displacement rate at the end of the hold period and  $\dot{P}_u$  is the unloading rate, which in this investigation was constant for the entire unloading. The elastic stiffness is then used in place of the standard unloading stiffness in eqn (4).

### Strain rate sensitivity

Constant rate of loading (CRL) strain rate sensitivity (SRS) as defined by Mayo and Nix:

$$m = \frac{d[\log \sigma]}{d[\log \dot{\epsilon}]} \quad (6)$$

was used to examine the strain rate dependency of photo-softening and thermal softening.<sup>24</sup> The stress is defined as  $\sigma = P/A$  and the strain rate is defined as

$$\dot{\epsilon} = \left( \frac{1}{h} \right) \left( \frac{dh}{dt} \right) = \frac{d[\ln h]}{dt} \quad (7)$$

We replace the depth with Doerner and Nix's plastic depth<sup>33</sup>

$$h_p = h - \left( \frac{dh}{dP} \right) P. \quad (8)$$

For calculating the SRS, the stress and the strain rate at 150 nm were determined. The load value at 150 nm was taken from the linear regression of the load *versus* depth curve between 125 nm and 175 nm. Similarly, the strain rate was taken as the slope of the linear regression of  $\ln(h)$  *versus* time between 125 nm and 175 nm. These averages were taken to minimize point-to-point variations in the data affecting the instantaneous stress or strain rate. The stress and strain rate was calculated for every indent and the average of each was taken for each loading rate. This resulted in 5 distinct points per condition (reference, irradiation, elevated temperature) for each sample. The strain rate sensitivity can then be obtained from the slope of the linear regression through the  $(\log \dot{\epsilon}, \log \sigma)$  points.

## Results

### Nanoindentation load-displacement curves, hardness and modulus

Fig. 4 presents representative load-displacement curves for the high and low azo content specimens at the 3 environmental conditions and a loading rate of  $50 \mu\text{N s}^{-1}$ . The low azo content sample showed negligible change in load-depth profile between the irradiated and reference conditions, as can be seen in Fig. 4a. For the high azo content sample, the probe was observed to indent much further in irradiated conditions compared to the reference (see Fig. 4b). Also, this increased indentation depth for the irradiated high azo content sample was observed across the entire loading, hold, and unloading.

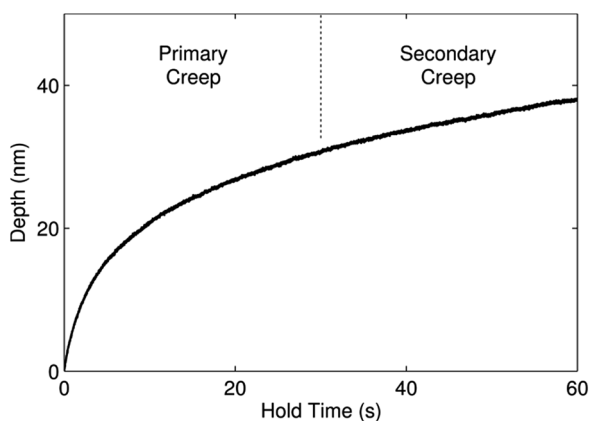


Fig. 3 Depth-hold time plot showing the two creep segments during the hold period. The hold period eliminates the significant creep observed during the primary segment, and allows the measurement of the near-linear secondary creep.

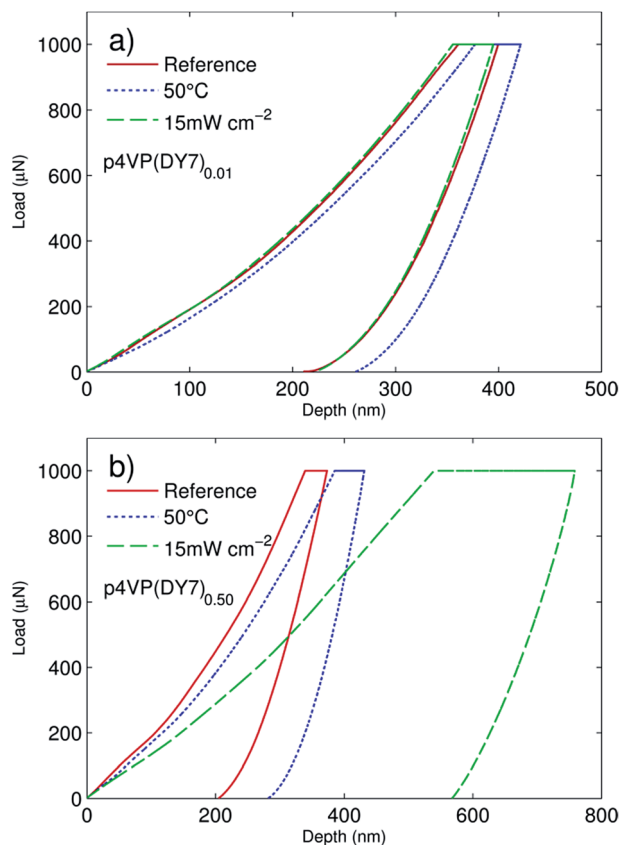


Fig. 4 The applied nanoindenter load as a function of depth for (a) p4VP(DY7)<sub>0.01</sub> and (b) p4VP(DY7)<sub>0.50</sub> for indents at 50  $\mu\text{N s}^{-1}$ . The photo-softening effect is apparent due to the significantly higher strain induced by the same load for the irradiated high azo sample. A more moderate softening effect is apparent in the elevated temperature indent.

This uniformity in behaviour for the entire load-unload cycle indicates that the light penetration remained near-uniform and there was no obstruction or shadowing of the light source by the indenter.

The trials at elevated temperatures descended further than the reference conditions in both samples (see Fig. 4a and b). However, the increased displacement for elevated temperatures was much less than that for the light exposed high azo content trial. This is especially true for the loading curve and hold segment, both portions of the test that are expected to be affected significantly by viscoplastic creep, if present.

The hardness is presented in Fig. 5. The hardness presented here is taken at the beginning of the hold period, to minimize the effect of the significant difference in hold period descent between environmental conditions. However, in the irradiated high azo sample, for which the creep is by far the most significant, there is still a large rate-dependency. It can be seen in Fig. 5 that a hardness decrease occurs in both the 0.50 and 0.01 azo samples at 50 °C. This hardness decrease below  $T_g$  has been observed in other amorphous polymers.<sup>34–36</sup> However, the hardness decrease in the 0.01 azo sample is smaller than in the 0.50 azo sample. It is likely that the intermolecular forces

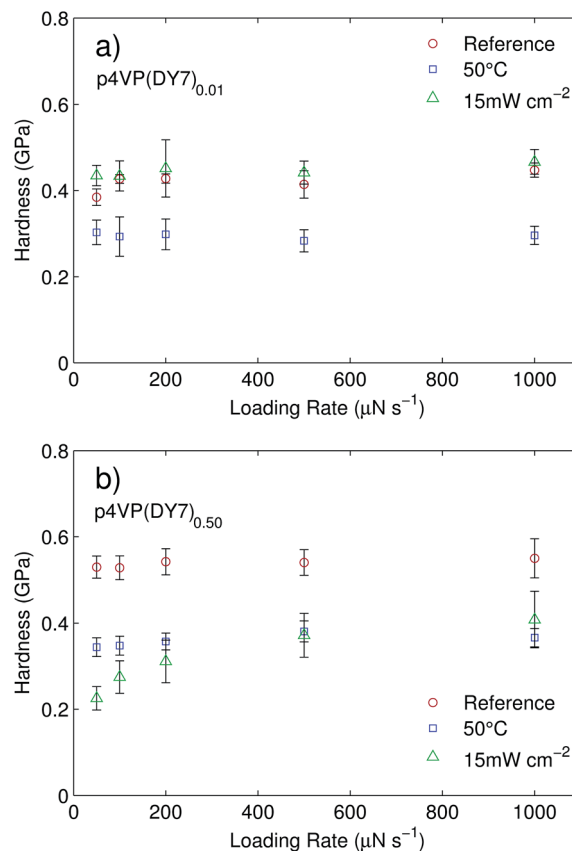


Fig. 5 Hardness at loading rates of 50, 100, 200, 500, 1000  $\mu\text{N s}^{-1}$  for (a) p4VP(DY7)<sub>0.01</sub> and (b) p4VP(DY7)<sub>0.50</sub>.

between DY7 chromophores largely contribute to the increased thermal softening effect. For the high azo content sample, the hardness differences indicate that the photosoftening effect is more significant than the thermal effect after slow loading rates. However, the significance is rate-dependent to the point that the magnitude of the decrease in hardness for the irradiated sample is smaller than the decrease for the thermal case. This rate-dependency points toward a strong viscoplastic effect being activated in the irradiated high azo content sample. Irradiating the low azo content specimen results in no significant change in hardness at any loading rates. The much smaller increase in plastic deformation for the elevated temperature samples can also be seen in Fig. 4.

The Oliver and Pharr moduli of both samples at various test conditions are depicted in Fig. 6. Averaged across all five loading rates, the mean creep-corrected elastic moduli at reference, elevated temperature, and irradiation conditions are 5.87, 5.47, and 5.59 GPa respectively for the low azo content sample. For the high azo content sample, the mean moduli are 5.24, 5.09, and 2.76 GPa respectively. It is apparent that there is a very slight elastic softening effect at elevated temperatures for both samples, but it can be seen that this effect is well within the bounds of one standard deviation of the reference and 50 °C trials. As expected, the high azo content sample under irradiation demonstrated a

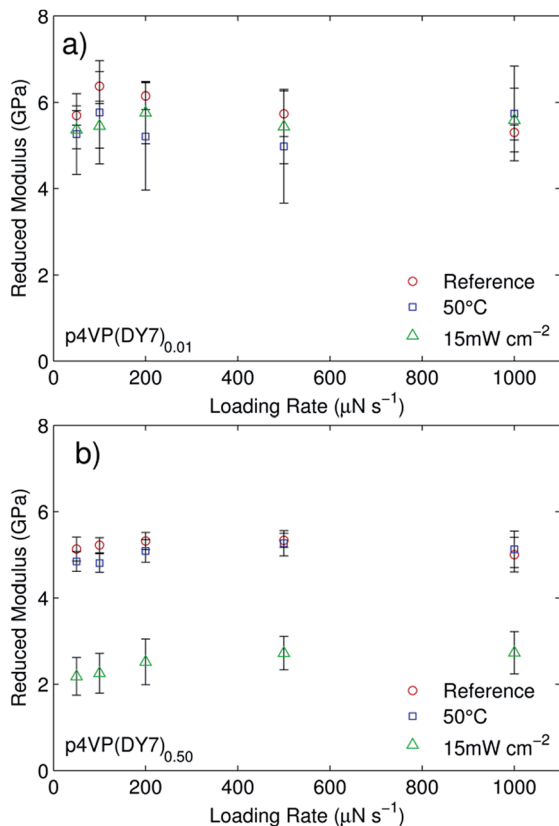


Fig. 6 The standard Oliver and Pharr reduced modulus at loading rates of 50, 100, 200, 500, 1000  $\mu\text{N s}^{-1}$  for (a) p4VP(DY7)<sub>0.01</sub> and (b) p4VP(DY7)<sub>0.50</sub>. A decreasing modulus with decreasing loading rate is visible for the 0.50 azo sample under irradiation, for which creep is significant.

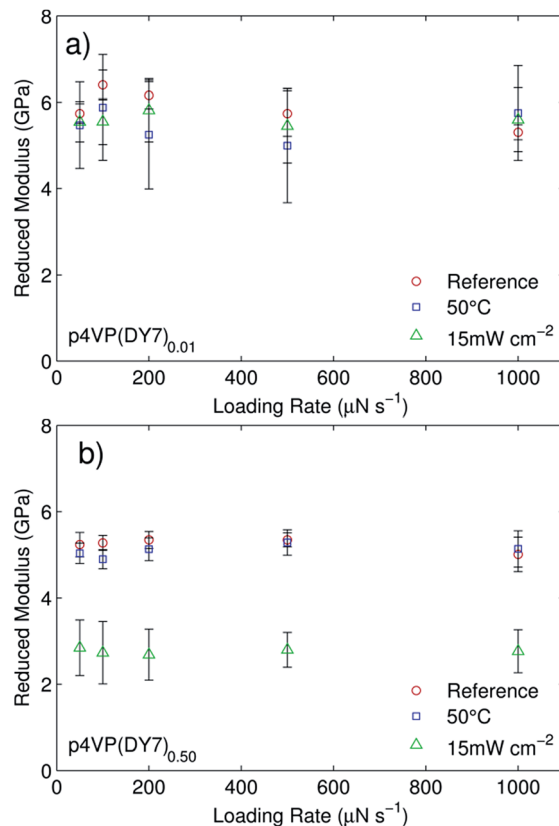


Fig. 7 The creep-corrected reduced modulus at loading rates of 50, 100, 200, 500, 1000  $\mu\text{N s}^{-1}$  for (a) p4VP(DY7)<sub>0.01</sub> and (b) p4VP(DY7)<sub>0.50</sub>.

significant photomechanical modulus decrease, far beyond the decrease observed when the specimens were tested at elevated temperatures.

### Comparisons between creep-corrected and Oliver and Pharr elastic modulus

Fig. 7 shows the results for the Ngan creep-corrected modulus. The results are reasonably similar to the Oliver and Pharr results in most cases. The 60 second hold was adequate for removing primary creep, and the effect of secondary creep resulted in a small effects, most readily observed for those tests with slow unloading rates where there is enough time in the unloading segment for the creep rate to be significant. High unloading rates resulted in the O&P and Ngan modulus being virtually identical. For the high azo sample, significant viscoplastic flow occurs and creep is a much more important factor. It can be seen in Fig. 6 that the O&P modulus is decreasing as the loading rate decreases. The creep-corrected modulus sees no such decrease. This is of particular importance as most studies examining azo-polymers focus on characterization of high azobenzene concentration samples, which demonstrate large mass transport and softening. This, coupled with the large creep in the irradiated sample, points to the necessity of

accounting for these effects in determining an accurate modulus.

### Constant rate of loading strain rate sensitivity

The stress-strain-rate data pairs are plotted in Fig. 8. The slope of the linear regression of the points, plotted on a log-log plot, is the strain rate sensitivity, and these values are presented in Table 1. The standard error was determined by root mean-squared deviation from the least-squares fit. As previous work by Vapaavuori and Mahimwalla *et al.* found, there is a significant increase in SRS for irradiated p4VP(DY7)<sub>0.50</sub>.<sup>21</sup> They showed the SRS increased by 123% from reference conditions to irradiated conditions. In our work, the increase from reference conditions was found to be 350%. The difference could be due to several factors. The loading rates examined by the previous study were lower than the loading rates examined by this study. It's also possible that the incident irradiation on the sample was different. Although the same light source was used a different indentation system was used and the angle of incidence may have been different, leading to a different fraction of azo activation directly below the indenter. Although the amount of change in strain rate sensitivity is different, the existence of a significant SRS change with light for both this study and that by Vapaavuori and Mahimwalla *et al.* demonstrates strain rate dependence to the photomechanical softening in supramolecular azobenzene-polymer complexes. Fig. 8 also demonstrates

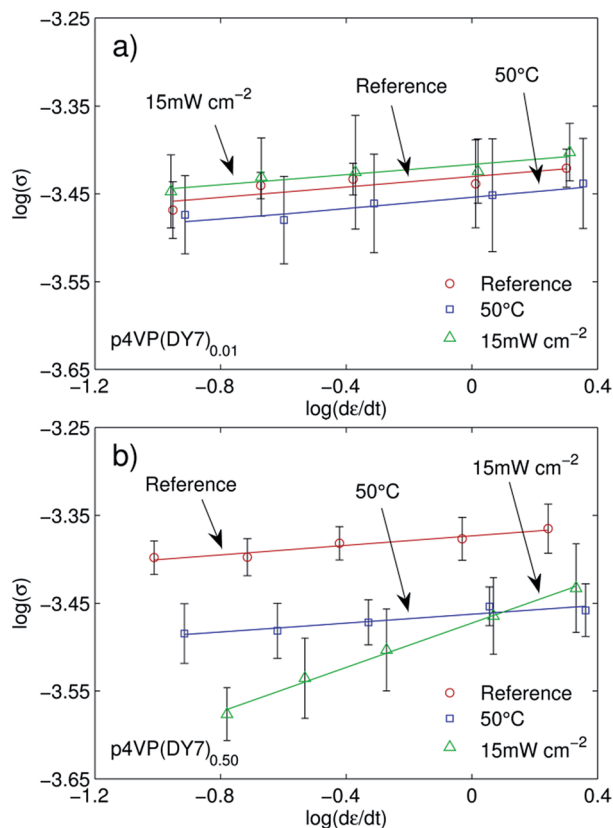


Fig. 8 The stress–strain rate data pairs for (a) p4VP(DY7)<sub>0.01</sub> and (b) p4VP(DY7)<sub>0.50</sub>. The slope of the linear regression in each data series is the CRL strain rate sensitivity. In the calculation of the stress, the depth was replaced with the plastic depth. There is negligible change in the sensitivity for all conditions, with the exception of the high azo content sample under irradiation.

Table 1 Constant rate of loading strain rate sensitivity of p4VP(DY7)<sub>0.01</sub> and p4VP(DY7)<sub>0.50</sub>

Experimental conditions	p4VP(DY7) <sub>0.01</sub>	p4VP(DY7) <sub>0.50</sub>
Reference	0.030 ± 0.011	0.028 ± 0.004
50 °C	0.029 ± 0.007	0.026 ± 0.006
15 mW cm <sup>-2</sup>	0.023 ± 0.007	0.126 ± 0.005

that there is negligible change in strain rate sensitivity at elevated temperature, indicating that the mechanism for thermal softening is different from that of photomechanical softening. However, in both figures it can be seen that the supported stress of the elevated temperature sample is lower than the reference samples, giving further evidence of the thermal softening mechanism.

## Discussion

The mechanical response for both samples under reference conditions is similar and exhibits little rate dependence. The plastic response (the hardness) and the elastic modulus are

similar between samples, although the added DY7 chromophores interestingly lead to a higher hardness, but a lower modulus. The small strain rate sensitivity in both samples is indicative of a very small viscoplastic effect, but the impact of these viscosity-driven effects on the hardness and modulus of both samples is negligible. The response of both samples indented at 50 °C, below  $T_g$  for both samples, was similar to that of the reference samples. The SRS was negligibly changed, as was the modulus. However, the samples demonstrated notably more plastic deformation, independent of rate.

The two samples under irradiation demonstrated markedly different behaviours. The irradiated high azo content sample showed a decrease in modulus, hardness, and an increase in strain rate sensitivity. In contrast, the low azo loading sample exhibited virtually no change from the reference condition for all properties (hardness, modulus, SRS) at all loading rates. The photsoftening of the high azo content polymer is a result of both a decrease in modulus and a significant viscoplastic flow component, as evidenced by the significant increase in strain rate sensitivity. This behaviour, as a photsoftening mechanism, is distinct from the mechanical property changes with applied temperature. It is clear, both from the changing strain rate sensitivity as well as the divergence between the Oliver and Pharr modulus and the creep-corrected modulus, that the photsoftening effect is fundamentally different from the thermal softening effect, where the softening was small, and has very little rate dependency and thus only a small viscoplastic component.

Significant viscoplastic flow leads to difficulty in obtaining a true modulus of elasticity. In this study, Ngan creep correction was used and found to be necessary for tests at slow loading rates. In Fig. 9, the divergence between the Oliver and Pharr modulus and the creep corrected modulus for the irradiated high azo sample is most clear at low loading rates.

This evidence of the activation of a creep mechanism is common in indentation-based studies of azo-materials, but its

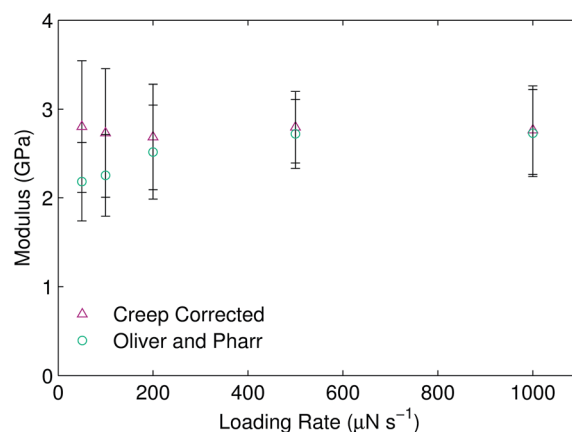


Fig. 9 The standard Oliver and Pharr modulus calculation method and Ngan's creep corrected modulus formulation for the irradiated high azo content sample. The creep leads to a strongly rate-sensitive modulus when calculated through the standard Oliver and Pharr model, even if a hold period is included.

effect is rarely accounted for in elastic modulus measurements.<sup>17,18</sup> The loading rate dramatically affects the creep time and therefore the magnitude of both the primary and secondary creep.<sup>37</sup> With rapid unloading, the effect of the secondary creep is minimized.<sup>38</sup> However, an increase in hardness has been observed at rapid loading rates.<sup>39–41</sup> The ideal loading profile for examining these parameters then is a slow loading rate and a rapid unloading, but this is dependent on how hardness is measured. Despite the impact of creep on the measured modulus, many studies examining softening in azo-polymers using nanoindentation rely solely on the Oliver and Pharr method.<sup>42–44</sup> In most studies, no hold period is used and often a visible ‘nose’ effect can be seen in the loading curves.<sup>18,45,46</sup> This problem can be further exacerbated by the use of higher intensity light sources, as the increased photodensity provides for more creep, resulting in a more dramatic ‘nose’ effect. Although to the knowledge of the authors the Ngan model has not been used to study azo-polymers, it has been successfully applied to amorphous polycarbonate and PMMA.<sup>47–49</sup>

In terms of general trends in mechanical properties, our work agrees with the pDR1m study undertaken by Karageorgiev *et al.*<sup>17</sup> Under 532 nm irradiation, they measured an elastic modulus of 0.9 GPa, as compared to a 3.4 GPa un-irradiated modulus. The magnitude of the modulus change measured is larger than ours – however, they used a more intense light source. They also noted that in the reference trials, the material behaved purely elastically up to a loading of 230 nN. However, when irradiated, there was no purely elastic region, even at loads below 30 nN. On their irradiated measurements there is a clear negatively sloped unloading curve, or ‘nose’. This photo-fluidization was expanded upon in the work of Fang *et al.*, in which they examine the transient local effective temperature of the azo chromophores during isomerization, and show the fluidization is comparable to a local temperature of 800 K – far above the applied temperature tested in our work, as well as the glass transition temperature.<sup>50</sup> The photofluidization effect, however, is not directly comparable to the described large heating effect. Indeed, our samples demonstrate little change in time-independent hardness, whereas at temperatures above  $T_g$  amorphous polymers are characterized by a steep decrease in hardness.<sup>34</sup> At rapid loading rates, the irradiated high azo sample has a hardness greater than that of the elevated temperature sample (see Fig. 5), indicating that the viscoplastic softening has a considerably larger impact than a time-independent plastic softening.

Modelling the mechanical properties of polymers with nanoindentation is a challenging undertaking. There are many recent papers detailing protocols such as that a Kelvin model, or modified/extended Kelvin model can be used with the indentation data.<sup>38,51–53</sup> These methods are most effective with bulk polymers. Here, with drop cast films, we have developed a simple nanoindentation method to extract both time-independent elastic modulus (*i.e.* the Ngan creep-corrected modulus) and a rate dependent parameter (*i.e.* the SRS), which is related to the viscoplasticity of the polymer. While this method does not provide the mathematical rigor of a Kelvin model, it is simple to implement and works on

both thin films and bulk polymers. It also addresses short-coming in previous work on azo-polymers that neglected to address the effect of viscoplasticity on the determination of the modulus of elasticity.

This combined viscoplasticity coupled with a time-invariant modulus change is distinct from both existing azo-polymer work, as well as examinations into other photoactive materials. Ma *et al.* model photomechanically-active polymers with a “photoviscoplastic” element in series with a combination of an elastic spring and a traditional Maxwell model in parallel.<sup>54</sup> Although they also note the change in the creep mechanism in the materials, the photoviscoplastic element fails to account for changes in time-independent elastic elements. However their model describes photo-induced network rearrangement in photoactivated covalent adaptive networks well, and so the active mechanism in azobenzene photo-activation must be driven by an activated creep mechanism (related to the plasticization observed by Karageorgiev *et al.* and Fang *et al.*) as well as a time-invariant elastic mechanism. Ikawa *et al.* proposed a series of steps explaining their observed surface patterning.<sup>55</sup> A photoisomerization induced softening of the polymer matrix followed by a polymer chain migration agrees well with our findings on both time-dependent and time-independent results. Indeed, their photo-induced surface patterning (viral patterning which uses a uniform irradiation, and is distinct from SRG formation) is evidence of a plastic (or viscoplastic) photsoftening far beyond what thermal effects could be responsible for.

## Conclusions

We have characterized the behaviour of azobenzene containing p4VP(DY7) at complexation degrees of 0.01 and 0.50 at ambient conditions, 50 °C, and under 15 mW cm<sup>-2</sup> 532 nm laser irradiation. Under irradiation, the high azo concentration sample demonstrated a large strain rate sensitivity increase, as well as a drop of roughly 50% in time-invariant elastic modulus. This is distinct from the thermal softening effect observed in the 50 °C trials, which demonstrated a rate-independent decrease in hardness, for both the low azo concentration sample and the high azo content sample. The elevated temperature trials however demonstrated no increase in strain rate sensitivity. These results indicate the mechanisms for photsoftening are different from thermal softening.

We have also demonstrated the importance of the creep-corrected elastic modulus model for nanoindentation as developed by Ngan *et al.* The increased strain rate sensitivity of the irradiated high azo sample causes significant creep which can lead to a reported elastic modulus far different than its true value, especially if the loading and unloading segments are slow. The confirmation and quantification of these photo-softening effects provided here can now be incorporated into numerical models of light-induced surface patterning, and associated optically driven flow observations in azo dye-containing polymer systems below  $T_g$ .

## Acknowledgements

JMH was supported in part by the NSERC USRA program, and wishes to thank Dr Thomas Singleton, Dr Jaana Vapaavuori, and Zahid Mahimwalla for assistance with experimental set-up and for providing the samples used in these experiments. This work was otherwise funded by NSERC Canada.

## Notes and references

- P. Rochon, E. Batalla and A. Natansohn, *Appl. Phys. Lett.*, 1995, **66**, 136–138.
- D. Y. Kim, S. K. Tripathy, L. Li and J. Kumar, *Appl. Phys. Lett.*, 1995, **66**, 1166–1168.
- N. K. Viswanathan, D. Y. Kim, S. Bian, J. Williams, W. Liu, L. Li, L. Samuelson, J. Kumar and S. K. Tripathy, *J. Mater. Chem.*, 1999, **9**, 1941–1955.
- R. Kirby, R. G. Sabat, J. Nunzi and O. Lebel, *J. Mater. Chem. C*, 2014, **2**, 841–847.
- A. Ambrosio, L. Marrucci, F. Borbone, A. Roviello and P. Maddalena, *Nat. Commun.*, 2012, **3**, 989–997.
- C. J. Barrett, J. Mamiya, K. G. Yager and T. Ikeda, *Soft Matter*, 2007, **3**, 1249–1261.
- C. J. Barrett, A. L. Natansohn and P. L. Rochon, *J. Phys. Chem.*, 1996, **100**, 8836–8842.
- A. Natansohn, P. Rochon, X. Meng, C. J. Barrett, T. S. Bonenfant and M. Pezolet, *Macromolecules*, 1998, **31**, 1155–1161.
- T. Pedersen and P. Johansen, *Phys. Rev. Lett.*, 1997, **79**, 2470–2473.
- M. L. Juan, J. Plain, R. Bachelot, P. Royer, S. K. Gray and G. P. Wiederrecht, *ACS Nano*, 2009, **3**, 1573–1579.
- P. Lefin, C. Fiorini and J. Nunzi, *Pure Appl. Opt.*, 1998, **7**, 71–82.
- D. Barada, M. Itoh and T. Yatagai, *J. Appl. Phys.*, 2004, **96**, 4204–4213.
- A. Leopold, J. Wolff, O. Baldus, M. R. Huber, T. Bieringer and S. J. Zilker, *J. Chem. Phys.*, 2000, **113**, 833–838.
- P. S. Ramanujam, M. Pedersen and S. Hvilsted, *Appl. Phys. Lett.*, 1999, **74**, 3227–3230.
- O. Baldus, A. Leopold, R. Hagen, T. Bieringer and S. J. Zilker, *J. Chem. Phys.*, 2001, **114**, 1344–1350.
- M. Saphiannikova, T. M. Geue, O. Henneberg, K. Morawetz and U. Pietsch, *J. Chem. Phys.*, 2004, **120**, 4039–4045.
- P. Karageorgiev, D. Neher, B. Schulz, B. Stiller, U. Pietsch, M. Giersig and L. Brehmer, *Nat. Mater.*, 2005, **4**, 699–703.
- A. Richter, M. Nowicki and B. Wolf, *Mol. Cryst. Liq. Cryst.*, 2008, **483**, 49–61.
- A. Ngan, H. Wang, B. Tang and K. Sze, *Int. J. Solids Struct.*, 2005, **42**, 1831–1846.
- K. G. Yager and C. J. Barrett, *J. Chem. Phys.*, 2004, **120**, 108910–108996.
- J. Vapaavuori, A. Priimagi and M. Kaivola, *J. Mater. Chem.*, 2010, **20**, 5260–5264.
- W. Oliver and G. Pharr, *J. Mater. Res.*, 1992, **7**, 1564–1583.
- I. N. Sneddon, *Int. J. Eng. Sci.*, 1965, **3**, 47–57.
- M. Mayo and W. Nix, *Acta Metall.*, 1988, **36**, 2183–2192.
- W. R. LaFontaine, B. Yost, R. D. Black and C. Li, *J. Mater. Res.*, 1990, **5**, 2100–2106.
- S. P. Baker, T. W. Barbee and W. D. Nix, *Mater. Res. Soc. Symp. Proc.*, 1991, **239**, 319–324.
- V. Raman and R. Berriche, *J. Mater. Res.*, 1992, **7**, 627–638.
- C. Huang, M. Wei and S. Lee, *Int. J. Plast.*, 2011, **27**, 1093–1102.
- G. Feng and A. Ngan, *Scr. Mater.*, 2001, **45**, 971–976.
- G. Feng and A. Ngan, *Mater. Res. Soc. Symp. Proc.*, 2000, **649**, 7.1.1–7.1.6.
- G. Feng and A. Ngan, *J. Mater. Res.*, 2002, **17**, 660–668.
- B. Tang and A. Ngan, *J. Mater. Res.*, 2003, **18**, 1141–1148.
- M. Doerner and W. Nix, *J. Mater. Res.*, 1986, **1**, 601–609.
- F. Ania, J. Martinez-Salazar and F. J. Baltá Calleja, *J. Mater. Sci.*, 1989, **24**, 2934–2938.
- O. A. Hasan, M. C. Boyce, X. S. Li and S. Berko, *J. Polym. Sci., Part B: Polym. Phys.*, 1993, **31**, 185–197.
- P. U. Veer, U. Pietsch and A. D. Mueller, *Appl. Phys. Lett.*, 2009, **94**, 231911–231914.
- B. Beake, *J. Phys. D: Appl. Phys.*, 2006, **39**, 4478–4485.
- S. Yang, Y. Zhang and K. Zeng, *J. Appl. Phys.*, 2004, **95**, 3655–3666.
- D. Peykov, E. Martin, R. R. Chromik, R. Gauvin and M. Trudeau, *J. Mater. Sci.*, 2012, **47**, 7189–7200.
- R. Schwaiger, B. Moser, M. Dao, N. Chollacoop and S. Suresh, *Acta Mater.*, 2003, **51**, 5159–5172.
- L. Shen, I. Y. Phang, L. Tianxi and K. Zeng, *Polymer*, 2004, **45**, 8221–8229.
- I. Tomatsu, A. Hashidzume and A. Harada, *J. Am. Chem. Soc.*, 2006, **128**, 2226–2227.
- M. Moniruzzaman, P. Zioupos and G. Fernando, *Scr. Mater.*, 2006, **54**, 257–261.
- M. Oyen, *Acta Mater.*, 2007, **55**, 3633–3639.
- M. Nowicki, A. Richter, B. Wolf and H. Kaczmarek, *Polymer*, 2003, **44**, 6599–6606.
- H. Zhang, X. Li and X. Wang, *Chin. J. Polym. Sci.*, 2010, **28**, 269–275.
- N. Fujisawa and M. V. Swain, *J. Mater. Res.*, 2008, **23**, 637–641.
- N. Fujisawa and M. V. Swain, *J. Mater. Res.*, 2006, **21**, 708–714.
- P. E. Mazeran, M. Beyaoui, M. Bigerelle and M. Guigon, *Int. J. Mater. Res.*, 2012, **103**, 715–722.
- G. J. Fang, J. E. MacLennan, Y. Yi, M. A. Glaser, M. Farrow, E. Korblova, D. M. Walba, T. E. Furtak and N. A. Clark, *Nat. Commun.*, 2013, **4**, 1521–1530.
- C. Huang, M. Wei and S. Lee, *Int. J. Plast.*, 2011, **27**, 10193–11102.
- L. Anand and N. M. Ames, *Int. J. Plast.*, 2006, **22**, 1123–1170.
- C. Y. Zhang, Y. W. Zhang, K. Y. Zeng and L. Shen, *J. Mater. Res.*, 2005, **20**, 1597–1605.
- J. Ma, Z. Mu, C. N. Bowman, Y. Sun, M. L. Dunn, H. J. Qi and D. Fang, *J. Mech. Phys. Solids*, 2014, **70**, 84–103.
- T. Ikawa, Y. Kato, T. Yamada, M. Shiozawa, M. Narita, M. Mouri, F. Hoshino, O. Watanabe, M. Tawata and H. Shimoyama, *Langmuir*, 2010, **26**, 12673–12679.